

# Intercomparison of IAGOS-CORE, IAGOS-CARIBIC and WMO/GAW-WCCOS Ozone Instruments at the Environmental Simulation Facility at Jülich, Germany

Herman G.J. Smit<sup>1</sup>, Torben Galle<sup>1,4</sup>, Romain Blot<sup>2</sup>, Florian Obersteiner<sup>3</sup>, Philippe Nédélec<sup>2</sup>, Andreas Zahn<sup>3</sup>, Jean-Marc Cousin<sup>2</sup>, Ulrich Bundke<sup>1</sup>, Andreas Petzold<sup>1</sup>, Valerie Thouret<sup>2</sup>, Hannah Clark<sup>2</sup>

<sup>1</sup> Institute of Climate and Energy Systems: Troposphere (ICE-3), Forschungszentrum Jülich (FZJ), Jülich, Germany.

<sup>2</sup> Laboratoire d'Aerologie, Université Toulouse III - Paul Sabatier, CNRS, Toulouse, France.

<sup>3</sup> Institute of Meteorology and Climate Research (IMK-ASF), Karlsruher Institut für Technologie (KIT), Karlsruhe, Germany.

<sup>4</sup> Previously published under the name Torben Blomel.

*Correspondence to:* Herman G.J. Smit (h.smit@fz-juelich.de)

**Abstract.** In the frame of the Quality Assurance (QA) plan of the In-service Aircraft for a Global Observation System (IAGOS), IAGOS-CORE and IAGOS-CARIBIC UV-photometer instruments have been compared with the dual-beam UV- Ozone (O<sub>3</sub>) PhotoMeter (OPM) of the World Calibration Center of Ozone Sondes (WCCOS) at the Forschungszentrum Jülich in an environmental simulation chamber. The WCCOS is established as part of the WMO-GAW measurement quality program of the global ozonesonde network for more than 30 years, in which the OPM instrument serves as the ozone reference standard. In the simulation chamber, pressure, temperature, and ozone concentration can be controlled at quasi-realistic flight conditions between the Earth surface (~1000 hPa) and ~35 km altitude (5 hPa). During the intercomparison, different ascent/descent and cruise altitude profiles of ozone, pressure and temperature have been simulated between the surface and ~12.5 km altitude (200 hPa).

In general, the two O<sub>3</sub> instruments P1-O3 (IAGOS-CORE) and CAR-O3 (IAGOS-CARIBIC) showed good agreement with the OPM reference standard within 5-6 %. At a pressure of 400-500 hPa the agreement was even within 2 %. The observed differences are small but systematic and reproducible during this experiment. CAR-O3 showed a small, but pressure independent deviation of  $-(1.5 - 2.5) \% \pm 1.5 \%$  compared to the OPM. P1-O3 revealed O<sub>3</sub> deviation to the OPM which changes with pressure of about +2% at 1000 hPa to -3% at 400 hPa, which might be an artefact on the experimental set-up and subject for further investigations. This intercomparison is a first step of the long-term goal to get the global ozone sonde data (GAW-NDACC-SHADOZ-GRUAN) and IAGOS-O3 (CORE: P1-O3, CARIBIC: CAR-O3) data traceable to one common reference, the OPM instrument of WCCOS. Recommendations are given for further regular validation of the flown instruments on external consistency in general and specifically towards the synergy of IAGOS-O3 and ozonesonde data. An important existing gap in doing intercomparison studies like this is that no ozone reference instrument is running at reduced pressures at any National Metrological Institute in the world. For the global observation networks of measuring free atmospheric ozone, it is essential to close this gap to enable the traceability of ozone measurements from different platforms to one reference standard, which is crucial to harmonize long-term ozone records to detect long term-changes of ozone in the free atmosphere.

## 1. Introduction

Ozone (O<sub>3</sub>) is both chemically and radiatively one of the most important trace gases in the atmosphere. It forms the stratospheric ozone layer shielding the Earth's surface from harmful UV sunlight (WMO/UNEP, 2023), while it is the major precursor of the hydroxyl radical (OH), the principal chemical detergent controlling the oxidation capacity (e.g. Thompson et al., 1992) and air quality in the troposphere (e.g. Cooper et al., 2014). Tropospheric ozone is also a potent natural and anthropogenically influenced greenhouse gas (IPCC, 2023). Monitoring the vertical ozone distribution on a regional as well as a global scale is essential for understanding long-term changes in both tropospheric and stratospheric ozone, as each may be affected by changes in the dynamics or chemistry of the atmosphere.

Besides the traditional balloon borne ozonesonde network (Smit et al., 2021) to sample tropospheric ozone, in the 1990's new ozone measuring platforms started their routine operations such as Lidar (e.g. McDermid et al., 1991; Ancellet et al., 1998), FTIR (e.g. Schneider et al., 2005; Vigoroux et al., 2008) and the in-service aircraft programs of MOZAIC (Measurement of OZone and water vapor by Airbus In-service airCRAFT) (Marenco et al., 1998a) and CARIBIC (Civil Aircraft for the Regular Investigation of the atmosphere based on an Instrumented Container) (Brenninkmeijer et al., 1999). Both in-service aircraft programs have been joined since 2011 into the IAGOS (In-service Aircraft in a Global Observing System) long-term monitoring programme (<https://www.iagos.org>; Petzold et al., 2015) as part of the European Research Infrastructure for global observations of atmospheric composition (Petzold et al., 2024). During normal scheduled flight operation, IAGOS measures in-situ ozone mixing ratios at cruise altitude (10-12.5 km) and provides vertical profiles of ozone from the surface to cruise altitude during take-off and landing. Since August 1994 and over more than 70,000 flights are archived in the IAGOS-database (<https://iagos.aeris-data.fr>). The data are widely used for climatological and trends analysis (e.g. Petetin et al., 2016; Cohen et al., 2018; Gaudel et al., 2020; Wang et al., 2022) as well as for model evaluations (e.g. Hu et al., 2017; Wagner et al., 2021).

Crucial for such long-term observations is to prove and monitor their long-term stability as well as the traceability of the instruments to a reference instrument on a regular basis. This can be done by checking the flown instruments on their internal and external consistency. The internal consistency of the IAGOS ozone instruments and their long-term measurements have been evaluated by Blot et al. (2021) and regular procedures have been developed to ensure the internal consistency over time. External consistency checks have been done in the past through in-flight comparison with ozonesonde measurements within a certain coincidence of space and time (Thouret et al., 1998; Staufer et al., 2013, 2014; Tanimoto et al., 2015; Tarasick et al. 2019; Wang et al., 2024). In general, over the entire period of more than 25 years of observations good agreement within 5-10% between the observing platforms has been achieved, whereby the ozone sondes consistently tend to measure about 5% more than the aircraft do.

In this study the external consistency of the IAGOS (CORE and CARIBIC) ozone UV photometer instrument has been investigated through intercomparison with the ozone photometer (OPM) of the World Calibration Centre of Ozone Sondes (WCCOS, <https://www.wccos-josie.org/en>) at the Forschungszentrum Jülich (FZJ) at their environmental simulation facility to calibrate airborne ozone and water vapor sensors. The WCCOS is established as part of the WMO-GAW measurement quality of the global ozonesonde network, whereby the OPM instrument serves as the ozone reference instrument. In the GAW-WCCOS simulation chamber, pressure, temperature, and ozone concentration can be controlled at quasi-realistic atmospheric conditions varying between 1000 hPa (surface) and 5 hPa (upper stratosphere) (Smit et al., 2000). The IAGOS-CORE O<sub>3</sub> instrument (here called "P1-O3") is part of the so-called IAGOS-CORE package P1 that is approved as EASA certified aeronautical equipment. Several Package P1 units are operated on commercial Airbus A340

and A330 aircraft (in 2024: 14 P1-units on 10 different aircraft of 8 international airlines). O<sub>3</sub> volume mixing ratio (VMR) measurements are performed for every flight from take-off to landing (cruise legs at about 180-250hPa). The tested CARIBIC instrument (here called “CAR-O3”) is part of the CARIBIC container laboratory and flown since 2010 on board an Airbus A340 by Lufthansa (Brenninkmeijer et al., 2007). This intercomparison is a first step of the long-term goal to get the global ozone sonde data (GAW-NDACC-SHADOZ-GRUAN) and IAGOS-O<sub>3</sub> (CORE: P1-O3 & CARIBIC: CAR-O3) data traceable to one common reference (OPM of WCCOS).

The key objective of the intercomparison is to investigate the performance of the three ozone UV-photometer instruments (OPM, P1-O<sub>3</sub>, CAR-O3) under controlled laboratory conditions in the ESC, thereby, simulating typical flight conditions of atmospheric pressure, temperature and ozone concentration between the surface and cruise altitude (Z=10-12.5 km). During the intercomparison different ascent/descent and cruise altitude profiles of ozone have been simulated. This paper presents and discusses the major results of the observed performance of the different instruments in quantitative terms. An outlook will be given on how to have ozone measurements of IAGOS and ozonesondes both traceable to one common ozone reference instrument, i.e. the OPM of the WCCOS chamber.

## 2. Experimental Details

### 2.1 Ozone UV-Photometer Instruments of IAGOS and WCCOS

The principle of the three UV-ozone photometer instruments involved in the intercomparison are based on the spectroscopic UV-absorption measurement of ozone at a wavelength around 254 nm in a well-defined sample chamber according to Beer-Lambert absorption law:

$$\ln\left(\frac{I_t}{I_o}\right) = -L \cdot \sigma_{O_3} \cdot C_{O_3} \quad (1)$$

where  $I_o$  (= zero mode) and  $I_t$  (=sample mode) are the lamp intensities at the detector when the chamber contains the sampled gas with and without removal of the ozone, respectively.  $L$  is the length of the absorption chamber,  $\sigma_{O_3}$  is the molecular absorption cross section of ozone at a wavelength of about 254 nm, and  $C_{O_3}$  is the average concentration of ozone in the absorption chamber. Since  $L$  and  $\sigma_{O_3}$  are well known quantities, and the transmittance  $R_t = I_t/I_o$  of the absorption chamber is determined by the ratio of the two observed signal intensities of the photo detectors in sample and zero mode, respectively, then the ozone concentration  $C_{O_3}$  can be derived (Eq.1). Through additional measurement of the pressure  $P_C$  and temperature  $T_C$  inside the absorption chamber the volume mixing ratio of ozone  $\mu_{O_3}$  can be derived from  $C_{O_3}$ .

$$\mu_{O_3} = -\frac{k}{L \cdot \sigma_{O_3}} \cdot \frac{T_C}{P_C} \cdot \ln\left(\frac{I_t}{I_o}\right) \quad (2)$$

whereby  $k$  is the Boltzmann constant

All instruments use the same widely applied UV-absorption cross-section ( $\sigma_{O_3} = (1,147 \pm 0.024) \times 10^{-17} \text{ cm}^2 \text{ molecule}^{-1}$ ) determined by Hearn (1961). In 2025 a new cross-section ( $\sigma_{O_3} = (1,1329 \pm 0.0035) \times 10^{-17} \text{ cm}^2 \text{ molecule}^{-1}$ : CCQM.O3.2019 (<https://www.bipm.org/en/gas-metrology/ozone>), by Hodges et al., 2019) will be introduced in the global ozone ground-

111 based monitoring networks (CCQM-GAWG, 2024) which is about 1.29 % lower, however, this will have no impact on the  
112 results of the present intercomparison.

113 All three ozone instruments are dual-beam UV-photometers that have two identical UV-absorption chambers (cuvettes),  
114 each alternating between reference mode (ozone-free air generated by directing it through an ozone scrubber being  
115 CuO/MnO<sub>2</sub>) and sample mode. A valve assembly alternates the scrubbed air between the two chambers, such that one  
116 chamber is in null mode while the other chamber is in sample mode or vice versa. The mode alternation compensates for  
117 changes in the light transmission through the cuvettes (e.g. due to temperature driven mechanical changes or changes of  
118 the reflectivity of the cuvettes due to changing surface coatings) and finally doubles the measurement frequency. Although  
119 the principle of operation is similar for all three photometer types, the instrumental layouts have significant differences.  
120 Specifications of the P1-O3, CAR-O3 and OPM ozone UV-photometer instruments participating in the intercomparison  
121 are summarised in Table 1. In general, the overall instrumental relative uncertainty is predominantly determined by the  
122 uncertainty of  $\sigma_{O_3}$ , the molecular absorption cross-section of ozone. For in-situ atmospheric measurements, however, also  
123 the sampling uncertainty must be considered that is dependent on the design of the air sampling (use of pump in inlet line  
124 or not), the use of proper material (e.g. PTFE) to avoid ozone losses at the walls, and the thermal concept and the electronic  
125 design. Therefore, regular pre- and post-flight tests and characterization of the instruments are essential.

#### 126 **2.1.1 GAW-WCCOS Ozone Photometer (OPM)**

127 The dual-beam UV-absorption ozone photometer (OPM) of the WCCOS serves as the reference instrument. It was  
128 developed by Proffitt and McLaughlin (1983) for use on stratospheric balloons. The overall uncertainty is  $\pm 2\%$  at P=1000-  
129 10 hPa. The instrument serves as reference (standard) of the GAW global ozonesonde network. The OPM is enclosed in a  
130 Styrofoam box, mounted inside a cylindrical vacuum tank which is connected to the simulation chamber and thus operates  
131 at the same pressure level as inside the simulation chamber. Details of the instrument and the data processing, including  
132 uncertainty budget are described in Proffitt and McLaughlin (1983).

133 No ozone reference instrument running at reduced pressures exists at any NMI (National Metrological Institute) in the  
134 world. This means that before and after the intercomparison, the OPM could only be compared at laboratory pressure  
135 conditions (1000 hPa) with a commercial, NIST-traceable “surface” ozone UV photometer of Thermo Electron Instruments  
136 (Model TEI-49) at volume mixing ratios between 0 and 200 ppbv. The agreement was within  $\pm 1$  ppbv below 100 ppbv  
137 and  $\pm 1\%$  above. No systematic bias was observed. Validation of the performance of the OPM at reduced pressures could  
138 only be done based on the evaluation of the measured physical parameters of the OPM as described in Proffitt and  
139 McLaughlin (1983).

#### 140 **2.1.2 IAGOS-CORE Ozone Instrument (P1-O3)**

141 The ozone monitor P1-O3 in IAGOS-CORE is a modified dual beam UV-photometer of Thermo Scientific (Model 49i)  
142 integrated together with a CO-infrared monitor in a special aeronautic flight box (Nédélec et al., 2015). The P1-O3  
143 monitor measures ozone at cabin air pressure conditions. Hereby, one UV-absorption cell is in measuring-mode and the  
144 second cell is in zero-mode. In zero mode the ozone is removed from the sampled air by an ozone scrubber (MnO<sub>2</sub>-  
145 catalyst filter) before the air sample enters the cell that is in zero-mode. Alternating, every 4 seconds (3 s for air flushing  
146 the cells and 1s for the measurement), the cells are switched from sample into zero-mode and vice versa. The pressure

147 and temperature in the absorption cells are measured to derive the ozone volume mixing ratio from the measured amount  
148 of light absorbed by ozone using Beer's absorption law.

149 In-flight ambient air is sampled through a forward-facing pitot tube and thereafter compressed by the Pump Box up to  
150 cabin air pressure and then led into the manifold at the inlet of P1-O3 splitting the total air flow into the nominal sample  
151 flow of 4 vol-l/min required for the O<sub>3</sub> and CO monitors and an excess flow, respectively. Thereby, the excess air flow is  
152 continuously monitored to ensure that the minimum required volume-flow of Pump Box (25 vol-l/min at ground, 5 vol-  
153 l/min at cruise altitude) is obtained. To avoid any losses of ozone due to physical and chemical interactions on the walls  
154 of the sampling lines, the pitot inlet tube and the interior of the pumps of the Pump Box are coated with PTFE, while all  
155 tubing are made of PTFE too.

156 Before and after aircraft operation (or each ~6 months, respectively), each P1-O<sub>3</sub>-instrument is checked (without the  
157 Pump Box) against a Thermo Scientific model 49PS reference instrument at several concentration levels to evaluate the  
158 instrument is responding linearly to ozone within 1 %. In addition, each P1-O<sub>3</sub> instrument is sent once a year to the  
159 French Laboratoire National d'Essais (LNE) for comparison with an instrument with measurements traceable to the  
160 National Institute of Standards and Technology (NIST). The overall uncertainty is better than  $\pm 2$  ppbv for O<sub>3</sub> < 100 ppbv  
161 and  $\pm 2$  % for O<sub>3</sub>  $\geq$  100 ppbv. (Nédélec et al., 2015).

162 Each flown P1-Package (P1-O<sub>3</sub> plus Pump Box) for IAGOS-CORE is compared before and after flight periods with the  
163 same MOZAIC-Rack as standard since the beginning of the program. Therefore, it is possible to remove systematic  
164 biases in the long-term time series and the resulting measurement uncertainty should represent only the contribution from  
165 random errors (Blot et al, 2021). More details of Package IAGOS-P1 (Pump Box and P1-O<sub>3</sub> instrument) and its  
166 operation are given by Nédélec et al. (2015) and Blot et al. (2021).

### 167 **2.1.3. IAGOS-CARIBIC Ozone Instrument (CAR-O3)**

168 The IAGOS-CARIBIC (CAR-O3) UV-photometer ozone instrument is fully custom-made and likewise applies a dual  
169 beam configuration. In zero-mode the ozone is removed using a MnO<sub>2</sub>-scrubber controlled at 38°C for maximum  
170 efficiency of 100%. Two three-way valves toggle each 4s to guide sample air and zero air alternatively between the two  
171 sample cuvettes. Each measurement takes 2 s and is preceded by flushing the cells for 2 s.

172 In contrast to commercial ozone monitors, the instrument uses a UV-LED (Seti, TUD59H1B) as a light source (see  
173 section 2.1 of Zahn, 2016). The LED light is guided into the two sample cuvettes (to ~47% each) using a beam-splitter.  
174 The remaining 6 % is measured by the opposing reference diode to actively control the LED (further stabilized at 20°C  
175 using a Peltier-element) to constant light emission with an uncertainty of  $\sim 10^{-4}$  (which is not possible with the  
176 conventionally used low-pressure Hg discharge lamps). However, since the UV-LED emission spectrum has a full-width  
177 half-mean (FWHM) of ~11 nm and may age, it is initially calibrated against a reference UV photometer and thereafter  
178 regularly cross-checked (about every 3 months).

179 Two photodiodes (Hamamatsu S1226) at the end of the cuvettes measure the UV light intensity using a two-channel (not  
180 multiplexing) 24-bit sigma-delta amplifier. Temperature is measured on the outside and the inside of the cuvettes.  
181 Pressure is measured directly at the exhaust of the cuvettes. Sample flow during aircraft operation of CAR-O3 is  
182 determined by the ram-pressure through the CARIBIC inlet system. This guarantees a minimum flow of 1.5 vol-l/min at  
183 cruise altitude. During the experiments reported here (without the ram-pressure on aircraft), a flow of ~2 vol-l/min was

184 enforced by a pump downstream of the instrument in combination with a needle valve for manual control of the flow.  
 185 The main specifications are listed in Table 1. Further details of handling and data processing are described in Zahn  
 186 (2016) as well as Obersteiner (2024, <https://doi.org/10.5281/zenodo.11104076>).  
 187 The measured precision (1-sigma) is 0.06 ppb at 1000 hPa and the response time of 4s. A simple calculation based on the  
 188 photon flux reaching the photodiodes (inferred from its photosensitivity and the measured photo current) and the detected  
 189 photo current noise indicate that this precision exactly agrees (to within 10-15 %) with the measured shot noise, that is,  
 190 CAR-O3 is quantum-noise limited and higher precision can only be reached with a stronger UV-LED or a longer  
 191 absorption (cuvette) length.  
 192 The total uncertainty of 2 ppb or 2% (whatever is higher) is dominated by the uncertainty of the O<sub>3</sub> cross section around  
 193 255 nm (Zahn, 2016). CAR-O3 is regularly (typically each 3-4 months) compared in the laboratory with a working  
 194 standard and once a year with a 2.7 m long-path UV photometer (by UMEG).

195

196 **Table 1. Specifications of the P1-O3, CAR-O3 and OPM ozone UV-photometer instruments participating in the**  
 197 **intercomparison.**

198

Property	P1-O3 IAGOS-CORE	CAR-O3 IAGOS-CARIBIC	OPM GAW-WCCOS
Light Source	Hg-Lamp (254 nm)	UV-LED (near 254 nm)	Hg-Lamp (254 nm)
UV Abs. Length	38 cm	38 cm	40 cm
Pressure	Cabin air	Ambient air	Ambient air
Inlet	Pitot (forward) + Compressor	Pitot (forward) + ram-pressure	N/A
Sample Volume Flowrate	24 l/min ( 2 l/min for P1-O3 & 2 l/min for P1-CO )	2 l/min	8 l/min
Response Time	4 seconds	4 seconds	2 seconds
Precision < 100 ppbv ≥ 100 ppbv	± 1 ppbv ± 1 %	± 0.1 ppbv ± 0.1 %	± 1 ppbv ± 1 %
Overall Uncertainty < 100 ppbv ≥ 100 ppbv	± 2 ppbv ± 2 %	± 2 ppbv ± 2 %	± 2 ppbv ± 2 %
Reference	Nédélec et al., 2015	Zahn, 2016	Proffitt and McLaughlin, 1983

199

## 200 2.2. Environmental Simulation Facility: GAW-WCCOS

### 201 2.2.1 GAW-WCCOS Simulation Chamber

202 The GAW-WCCOS simulation chamber established at the Forschungszentrum Jülich (FZJ) is designed to investigate the  
 203 performance of different types of balloon-borne ozone sensors as well as airborne humidity sensors to measure the vertical  
 204 distribution of atmospheric ozone and water vapor, respectively (Smit et al., 2000). The key component of the facility is a

simulation chamber with a test room volume of about 500 liters (80x80x80 cm) whose pressure as well as temperature can be dynamically regulated between 5 and 1000 hPa and between 200 and 300 K at temperature rates between -2K/min and +5K/min. The volume mixing ratio of ozone can be dynamically regulated between 5 and 10000 ppbv to simulate typical atmospheric ozone levels between the surface and 35 km altitude. Since 1994, the facility has been established as the World Calibration Centre for Ozone SondeS (WCCOS) as part of the QA/QC-management plan of the Global Atmosphere Watch (GAW) program of the World Meteorological Organization (WMO). In the scope of this framework since 1996, international JOSIE (Jülich Ozone Sonde Intercomparison Experiment) campaigns have been conducted to assess the performance of the major types of ozone sondes used within the global network of ozone sounding stations (Smit et al., 2007, 2024; Thompson et al., 2019). The dual beam UV-photometer OPM (section 2.1.1) serves thereby as an ozone reference. The entire simulation process is automated by computer control to guarantee reproducible ambient conditions. JOSIE observations have demonstrated that the experimental set-up of the WCCOS simulation chamber experiment has a reproducibility of about  $\pm 1\%$ . Details of the facility and its use as WCCOS are given by Smit et al. (2000).

### **2.2.2 Ozone Profile Simulator (OPS)**

The Ozone Profile Simulator (OPS) unit of GAW-WCCOS (Smit et al., 2000) is used to simulate reproducible pressure dependent ozone profiles dynamically in time. Therefore, a separate gas mixing system is installed to supply equivalent air samples to up to four ozone sensors plus the UV-photometer (OPM) with pre-set ozone concentrations. Ozone is photolytically generated by UV-irradiation in a zero-grade airflow through a quartz glass (Suprasil) tube using a low-pressure Hg-discharge lamp. Via the photodissociation of oxygen molecules at a wavelength of 185 nm ozone is formed at high levels of 0.1-0.2 % at a constant flow of 50 cm<sup>3</sup>/min through the quartz glass cell (pressurized at 4000 hPa, volume: ~40 cm<sup>3</sup>). To vary the ozone volume mixing ratio between 10 and 10000 ppbv at different air pressures, the high-ozone airflow is dynamically diluted by a two-staged mixing with zero-grade air flows. All air flows are regulated by mass-flow controllers (Smit et al., 2000). The air used is dried and purified such that any sensitivities of the UV-Photometers to humidity or sudden changes of it (Wilson and Birks, 2006) can be excluded. The sample flow is connected to a glass manifold inside the simulation chamber to feed the different O<sub>3</sub>-instruments, whereby excess air can flow via an exhaust, such that the inlet tubes of all connected instruments are at the same pressure condition as inside the WCCOS-chamber.

## **2.3 Experimental Design Intercomparison**

### **2.3.1 Experimental Setup**

The schematic of the experimental setup is shown in Figure 1. Ozone-containing air is produced in the OPS and fed into a gas manifold located inside the simulation chamber. The inlet tubes of the three ozone instruments are connected to the manifold via gas-feed through (all made of PTFE). CAR-O<sub>3</sub> uses a 2 m tube (ID = 4 mm), while the P1-O<sub>3</sub> the inlet line goes via the P1-Pump Box that compresses the sample air to cabin or (here) laboratory pressure before entering the P1-O<sub>3</sub> instrument. The OPM, mounted in a vacuum tank connected to the simulation chamber, is at the same pressure condition as inside the chamber.

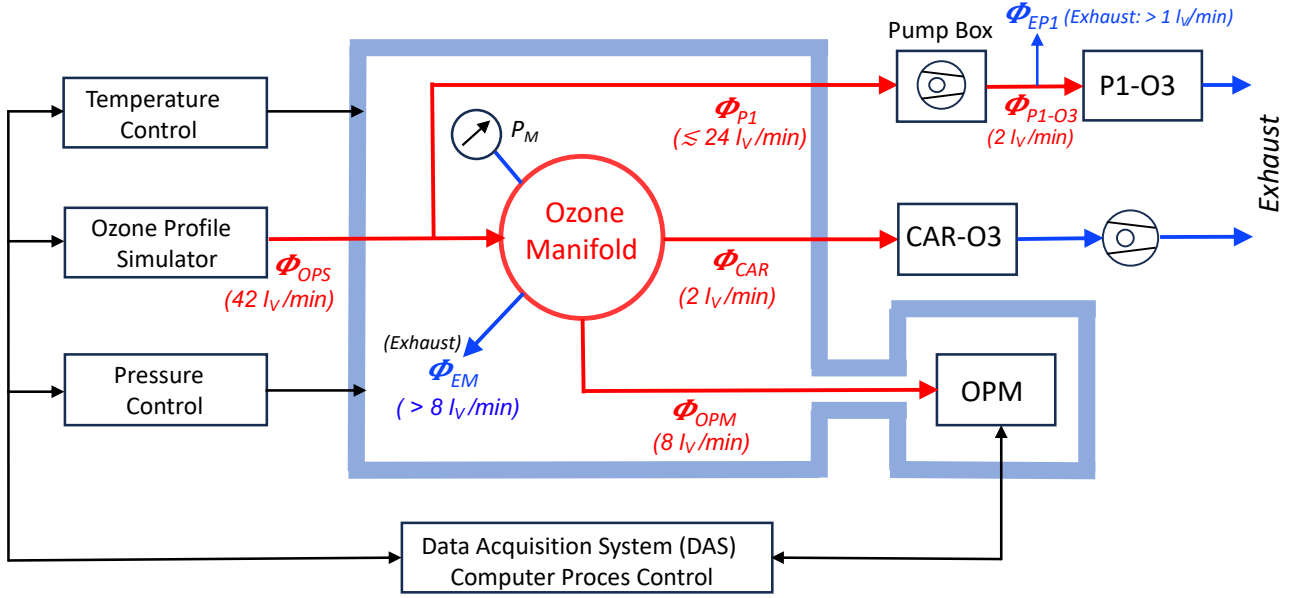


**Figure 1: Schematics of the experimental setup for the intercomparison at the WCCOS, showing the ESC with OPM of the WCCOS, the connection to the IAGOS-CORE and IAGOS-CARIBIC ozone instruments, the ozone manifold located inside the simulation chamber and its control systems, including the computer-controlled DAS.**

The sample manifold consists of a spherical glass vessel with a volume of about 150 cm<sup>3</sup> with radially arranged connections to the individual ozone instruments with the inlet of the simulated ozone air flow  $\Phi_{OPS}$  being in the centre of the manifold. Excess air is exhausted via an additional tube such that the manifold is kept to the sample volume pressure (measured by a pressure sensor) and to prevent the inlet lines of the ozone instruments from overpressure effects that may cause measurement artefacts.

For the JOSIE experiments (for testing ozone sondes), the volume flow rate of the simulated ozone air flow  $\Phi_{OPS}$  is kept constant at 12 vol-l/min which is sufficient to provide four ozone sondes (maximum 4 x 0.25 vol-l/min) and the OPM (maximum 8 vol-l/min). For the IAGOS-ozone intercomparison, higher flow rates were required, see instrument sample flows in Table 1. The total volume flow rate is at least 36 vol-l/min. To ensure a significant exhaust flow at the manifold, we thus increased the typical volume flow of 12 vol-l/min by an additional 30 vol-l/min flow controller to obtain a total volume flow  $\Phi_{OPS}$  of 42 vol-l/min and thus an exhaust flow of the manifold of 6 vol-l/min (Fig.1). The pressure  $P_M$  inside the manifold was monitored to ensure to keep it a few hPa higher than the pressure in the test chamber itself to avoid any leakage effects of air from the chamber into the manifold. The P1-O3 sample flow we had to branch off from the ozone profile simulator flow before entering the manifold (Fig.1), because it was shown that the high sampling volume rate of P1-O3 pump box would otherwise cause leakage effects when P1-O3 was directly connected with a Teflon fitting at the inlet glass tube of the manifold.

### 2.3.2 Simulation of Realistic Flight Conditions

It is essential to operate the chamber at appropriate pressure conditions to simulate realistic flight conditions that the IAGOS instruments experience when connected to the air inlets. Both air-sample inlets (of IAGOS-CORE and IAGOS-CARIBIC) are facing forwards and thus use the dynamic (ram) air pressure generated by the high speed of the aircraft. On IAGOS-CARIBIC a special inlet configuration hinders (aerosol and cloud) particles larger than ~2 μm to enter the sampling line. At the maximum cruise altitude of about 12.5 km, the lowest static air pressure is 180 hPa at a typical aircraft speed of



264 Mach = 0.81+/-0.02 causing an adiabatic compression factor of about 1.6. In an ideal case, this leads to a dynamic ram air  
265 pressure of about 100 hPa. However, in practice some pressure losses of about 30 hPa have to be considered, such that the  
266 lowest total air pressure inside the inlets is about 250 hPa. Note, however, as P1-O3 runs a pump to compress sampled air  
267 to cabin pressure (here laboratory pressure) before entering P1-O3 instrument, the pressure ranges of P1-O3 and CAR-O3  
268 covered by our tests are different, but for both instruments span the relevant pressure ranges between surface and cruise  
269 altitude.

270

#### 271 A. IAGOS-CORE = P1-O3

272 The P1-Pump Box supplied with sample air from the forward-facing inlet system compresses the sampled air to cabin air  
273 pressure. The cabin air pressure is prescribed by civil aviation regulations to be above 750 hPa and usually ranges at 800-  
274 850 hPa at cruising altitude. In-flight, the maximum pressure difference between cabin and the inlet of P1-PU thus is 850-  
275 250 = 600 hPa. For the present laboratory intercomparison we thus must cover the pressure range between 1000 hPa and  
276 400 hPa (= 1000 - 600 hPa).

277

#### 278 B. IAGOS-CARIBIC = CAR-O3

279 The CAR-O3 instrument does not use a pump, and its inlet pressure is the ambient static pressure, plus the ram-pressure  
280 minus some pressure loss in the sampling line (see above), that is, 250 hPa at maximum cruise altitude. To simulate the  
281 ram-pressure effect (exhaust at 180 hPa), during this laboratory intercomparison the CAR-O3 instrument does not use a  
282 pump at the exhaust to force an air flow of about 2 vol-l/min (Fig.1).

283

### 284 3 Results

#### 285 3.1. Introduction

286 Table 2 gives an overview of the simulation experiments performed. The first day (12 June 2023) was reserved for  
287 installation of the equipment and for a short test run to ensure proper functioning of equipment and data acquisition of the  
288 different instruments. On the second day (13 June 2023) another test of the P1-O3 and CAR-O3 instruments followed by  
289 sampling outside ambient air. The results of these two tests are beyond the scope of this report. The core of the  
290 intercomparison itself took place on 13 until 15 June 2023 with the four simulation experiments, numbered 3 to 7, which  
291 will be presented here in more detail.

292

293

**Table 2. List of intercomparison experiments performed during the IAGOS-WCCOS Ozone Intercomparison (IWOI) campaign between 12 and 15 June 2023 at WCCOS (FZJ/IEK-8, Jülich, Germany).**

Date	Exp. Nr & Sim. Nr	Profile Type	UTC-Time	Pressure (hPa)	Remarks
Day#1: 12-06-2023	#1 & 223	Test	13:00-15:00	1000-300	Installation and testing equipment
Day#2.1: 13-06-2023	#2 & NAN	Ambient Air (Day2.1_Ambient)	07:30-09:30	1000	P1-O3 & CAR-O3 & No OPM
Day#2.2: 13-06-2023	#3 & 224	Ascent-Cruise-Descent (Day2.2_Profile)	12:00-17:00	1000-400-400-1000	P1-O3 & CAR-O3 & OPM
Day#3.1: 14-06-2023	#4 & 225	Ascent-Cruise-Descent (Day3.1_Profile) Cruise: O3 Step-Up/Down	07:30-11:30	1000-400-400-1000	P1-O3 & CAR-O3 & OPM
Day#3.2: 14-06-2023	#5 & 226	Discrete Pressure Levels (Day3.2_Profile) Total OPS-Flow: 12 vol-l/min	11:30-14:00	1000-400-250	CAR-O3 & OPM & No P1-O3
Day#3.3: 14-06-2023	#6 & 226	Ascent-profile (Day3.3_Profile) Ascent Zero Ozone	14:00-15:00	1000-250	CAR-O3 & OPM & No P1-O3
Day#4.1: 15-06-2023	#7 & 228	Discrete Pressure Levels (Day3.3_Profile)	07:00-10:30	1000-400	P1-O3 & CAR-O3 & OPM

## 3.2 Comparison of P1-O3, CAR-O3 and OPM at a pressure of 400-1000 hPa

### 3.2.1 Experiment #3: Ascent-Cruise-Descent

Experiment #3 (numbering, see second column in Table 2) simulates an aircraft doing an “ascent - cruise altitude - descent” profile of pressure and ozone volume mixing ratio (Figure 2, 4, 5). The lowest pressure of 400 hPa is to simulate the maximum pressure difference the P1 pump box must achieve between cruise altitude and about 1000 hPa in the laboratory (see explanation in section 2.3.2.). In the first part of the simulation, during the ascent and the beginning part of the cruise phase, the ozone level was maintained at 400-500 ppbv to clean the inlet tubes of the OPM, P1-O3 (including P1-Pump Box) and CAR-O3 instruments. In the second part, the ozone was lowered to about 100 ppbv. The three missing data intervals of CAR-O<sub>3</sub>-instrument were caused by a malfunction of its temperature controller of the UV-LED light source such that the measured O<sub>3</sub> values were rejected and not shown in the graph and excluded from further analysis.

The relative differences in % of the  $\mu_{O_3}$  (VMR) readings of P1-O3 and CAR-O3, respectively, shown in this study are consequently defined with respect to the  $\mu_{O_3}$  readings of the OPM-O3 instrument acting as the reference as follows:

$$Rel. Difference of P1O3 = \frac{(\mu_{O_3, P1O3} - \mu_{O_3, OPMO3})}{\mu_{O_3, OPMO3}} \quad (3)$$

$$Rel. Difference of CARO3 = \frac{(\mu_{O_3, CARO3} - \mu_{O_3, OPMO3})}{\mu_{O_3, OPMO3}} \quad (4)$$

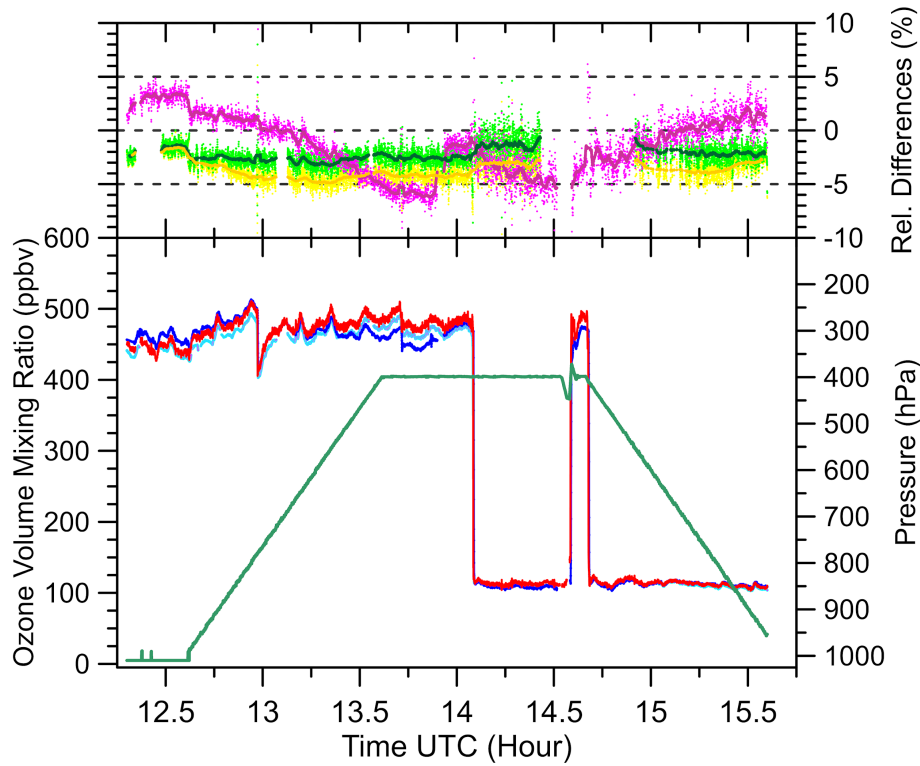


**Figure 2:** Experiment #3: Time-series of pressure (dark green) and ozone volume mixing ratio to simulate an ascent-cruise-descent track of an IAGOS aircraft for P1-O3 (blue), CAR-O3 (light blue) and OPM (red). The relative differences compared to each other are P1-O3 to OPM (magenta) and CAR-O3 (original: V1) to OPM (yellow) and CAR-O3 (pressure-sensor corrected: V2, see text) to OPM (light green). Fat solid lines are 3-minute running averages of the relative differences.

In general, the three instruments follow the simulated ozone profile well and agree among each other between -5 and +2% (Fig. 2). P1-O3 compared to the OPM shows a pressure dependence, that is, from +3% at 1000 hPa down to -5 % at cruise altitude conditions. The CAR-O3 instrument initially showed an increasing negative offset relative to the OPM of a 1% at 1000 hPa (at ~12:30) to -4 % at 800 hPa and lower pressures. This somewhat strange behaviour was subject to further investigations on the underlying cause. In a subsequent test (May 2024), KIT (Karlsruher Institut für Technologie), responsible for the operation of the CAR-O3 instrument, found an issue with the electronic analog-digital converter of the data acquisition card of CAR-O3 that generated a systematic 2.2% difference of the reading of the pressure,  $P_{Cuv}$  inside the absorption cuvettes below a pressure of ~800 hPa (see Figure 3a.). This electronic artefact has been eliminated and the pressure readings before and after the repair of the AD-converter were compared against an accurate reference pressure,  $P_{Ref}$ , sensor (Omega HHP360, accuracy: 0.25 hPa). The observed pressure differences,  $\Delta P_{Abs} = P_{Cuv} - P_{Ref}$  as function of the reference pressure  $P_{Ref}$  (Figure 3a.) are used to correct all original CAR-O3 data (version V1) into the new pressure-sensor corrected CAR-O3 data (version V2). After the repair of the AD-converter, the corrected V2 data show a rather constant, pressure independent, deviation of about -2 % compared to the OPM (Fig. 3b.) We only will present the pressure corrected CAR-O3 data. There exists just one single CAR-O3 instrument that is in flight operation. Meanwhile, all CARIBIC-Ozone data in the IAGOS database (<https://iagos.aeris-data.fr/>) have been corrected accordingly. For the two similar CAR-O3 type instruments (FAIRO-1 and FAIRO-2) which are flown on the German research aircraft HALO (HALO (High Altitude and Long-Range Research Aircraft) the ADC-cards were configured correctly, such that no correction is needed.

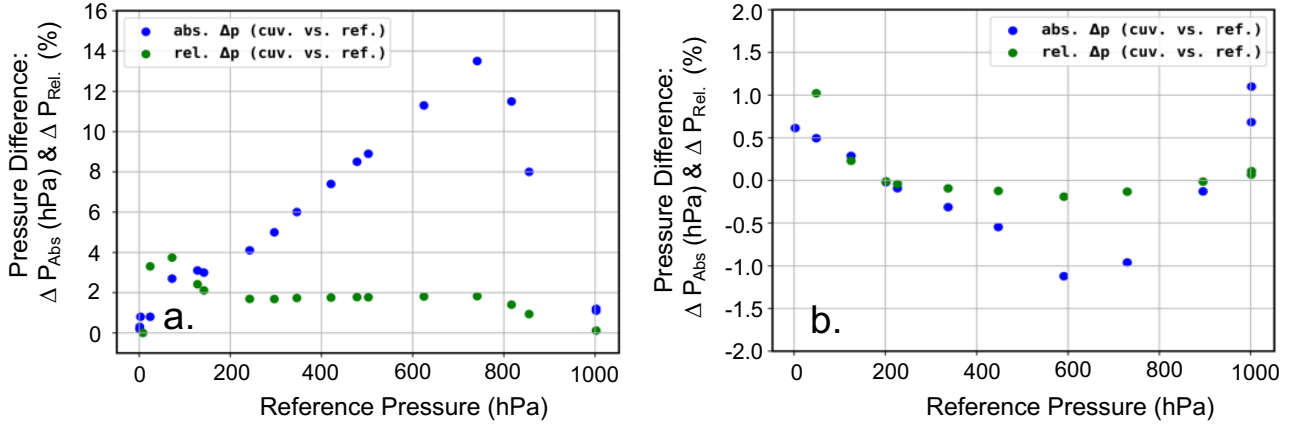


**Figure 3** Comparison of CAR-O3 air pressure sensor,  $P_{Cuv}$ , inside UV-absorption cuvette) against accurate reference pressure,  $P_{Ref}$ , sensor (Omega, HHP360, uncertainty: 0.25 hPa) before (left diagram a.) and after (right diagram b.) solving the electronic artifact of the AD-converter (details see main text). Displayed are the pressure differences  $\Delta P_{Abs} = P_{Cuv} - P_{Ref}$ , in hPa (blue dots) and their relative differences  $\Delta P_{Rel} = \Delta P_{Abs} / P_{Ref}$ , in % (green dots).

In Figure 4 the identical data (experiment No. 3, see Fig. 2) have been split into the vertical  $O_3$ -profiles during ascent (Fig. 4a) and descent (Fig. 4c) and the cruise altitude section at 400 hPa (Fig. 4b). The behaviour of P1-O3 and CAR-O3 described above occurs identically during ascent and descent, and no indication for any hysteresis effects could be observed. This is also confirmed by the fast responses of both instruments on the sharp upward or downward steps of the simulated ozone levels.

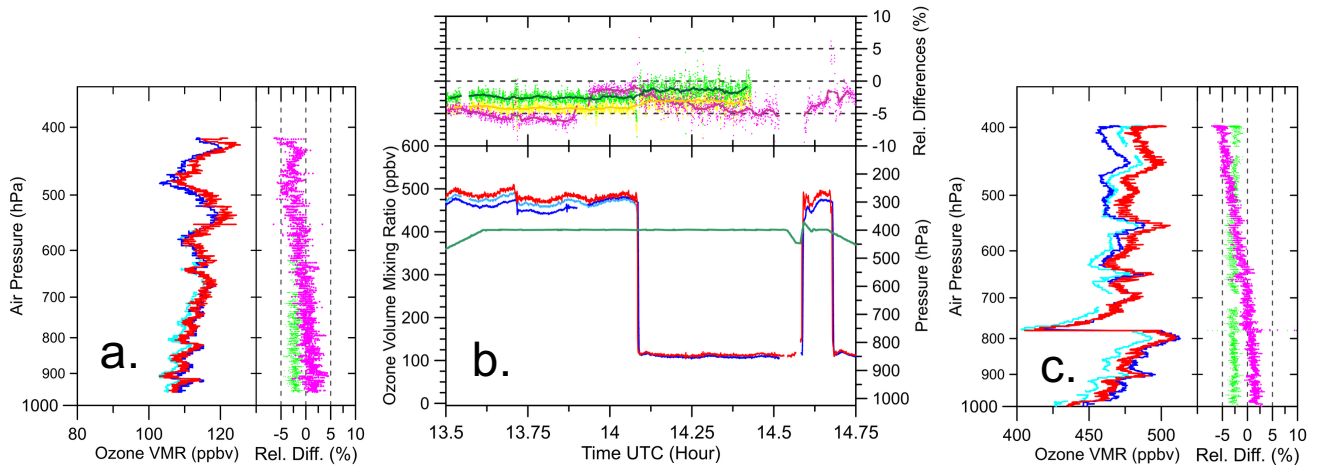


**Figure 4.** Experiment No. 3: Same data (and colours) as in Figure 2 but has been split into ascent (a: left diagram), cruise altitude (b: center diagram) and descent (c: right diagram). The measured ascent and descent profiles are displayed as ozone versus the simulated pressure ( $^{10}$ Log scale), while the cruise track part is plotted as time series.

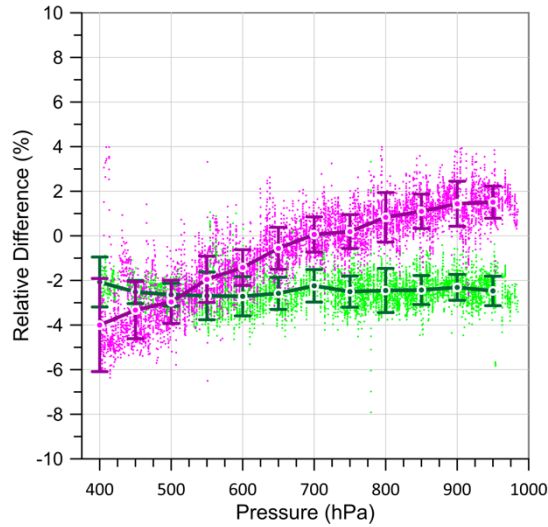


**Figure 5. Experiment No. 3: Same data (and colours) as in Fig. 2, but relative differences among P1-O<sub>3</sub>, CAR-O<sub>3</sub> and OPM as function of pressure. Thick solid lines are averages over 50 hPa pressure bins with their 1  $\sigma$ -standard deviation.**

The results of this Exp#3 are summarized in Figure 5 that displays the relative differences of P1-O<sub>3</sub> and CAR-O<sub>3</sub> compared to the OPM as scatter plot and function of the air pressure inside the chamber. The thick curves are the corresponding averages over 50 hPa bins with their one standard deviation.

### 3.2.2 Experiment #4: Ascent - Cruise (O<sub>3</sub> steps) - Descent

This simulation experiment is similar to Exp. No. 3, with the following differences: during ascent and descent the ozone volume mixing ratio was held at 110 ppbv, while at cruise altitude, the ozone was varied (stepped up and down) at different levels of 100, 250, 370 and 500 ppbv, see Figures 6 - 8 equivalent to the Figures 2, 4 and 5 respectively.

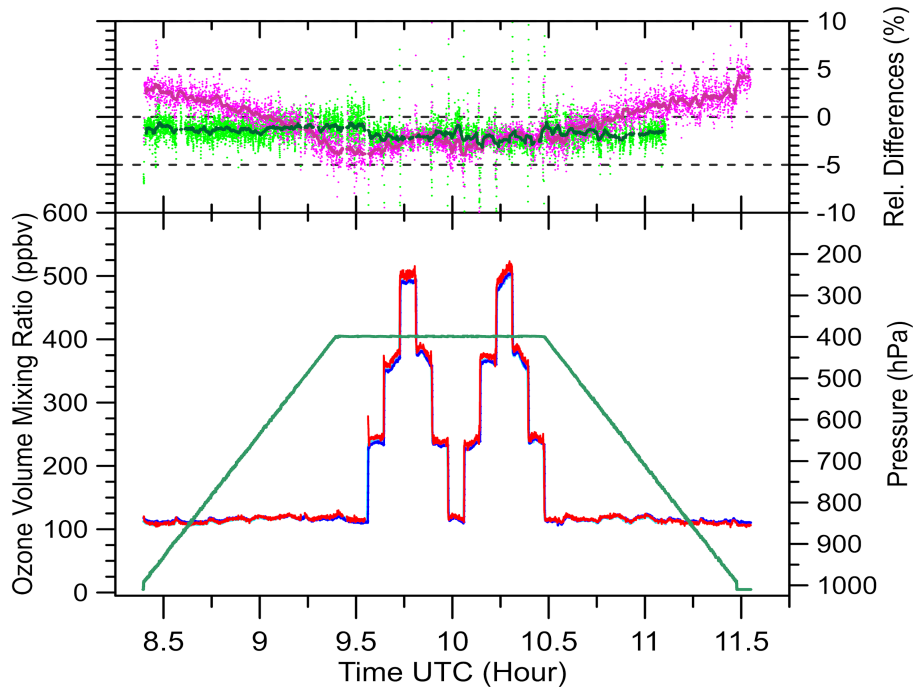
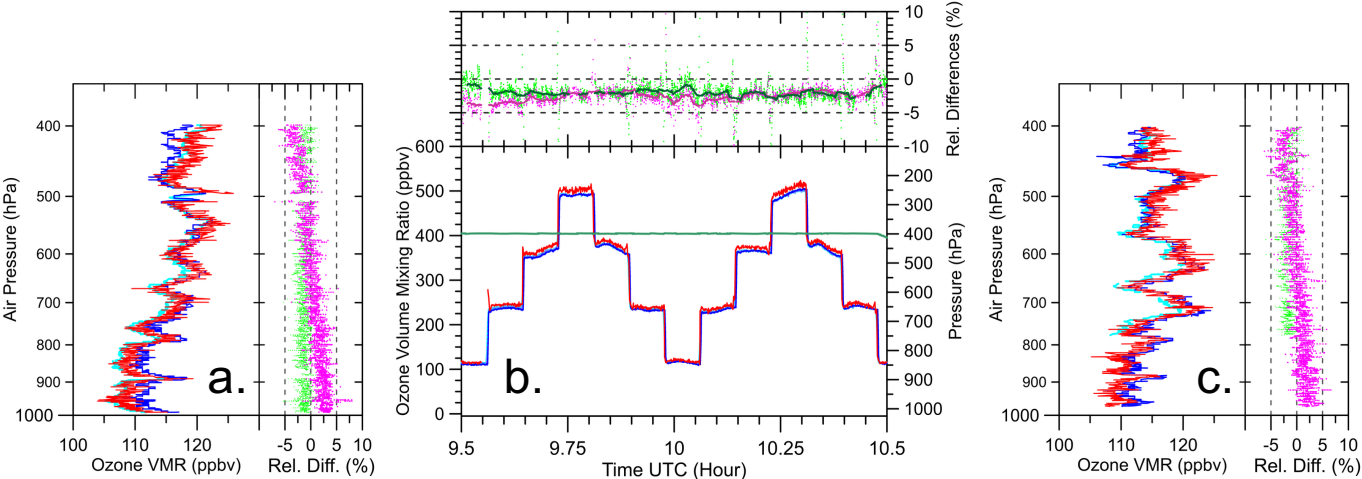


**Figure 6. Experiment No. 4: Graph and colour coding identical to Fig. 2.**

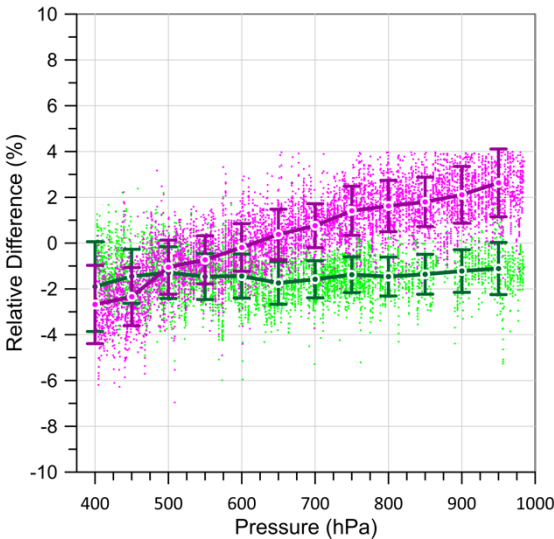
373  
374  
375  
376  
377  
378  
379  
380  
381  
382

Also, in this simulation experiment the instruments follow the simulated ozone profile well and agree among each other to within  $\pm 3\%$ . From Fig. 7 and 8 it is depicted that the P1-O3 compared to the OPM show a significant decrease with decreasing pressure, similar as in the previous Exp. No. 3 from +3% at 1000 hPa down to -3 % at 400 hPa (cruise altitude conditions). The CAR-O3 instrument relative to the OPM revealed a similar behaviour as in Exp. No. 3: - (1.5 – 2) % deviation that is constant at pressures between 1000 hPa and 400 hPa. Remarkable is that the span and slope of all data are identical to Exp. #3, but all data are shifted to (0.8 - 1.0) % higher values. Based on this observation we estimate the reproducibility of the experimental set-up within +/- 1%. Further, no indications are found on any memory or hysteresis effects for both instruments.



383  
384  
385  
386

**Figure 7. Experiment No. 4: Graphs and colour coding identical to Fig. 4.**



387  
388  
389  
390

**Figure 8. Experiment No 4: Graph and colour coding identical to Fig. 5.**

### 3.2.3. Experiment No. 7: O<sub>3</sub> Step Up/Down at Different Pressure Levels

In this simulation experiment at three different discrete pressure levels (950, 600 and 400 hPa) the ozone levels were varied (step up and down) at discrete values typically found at the corresponding pressure levels, (See Figures 9 and 10).

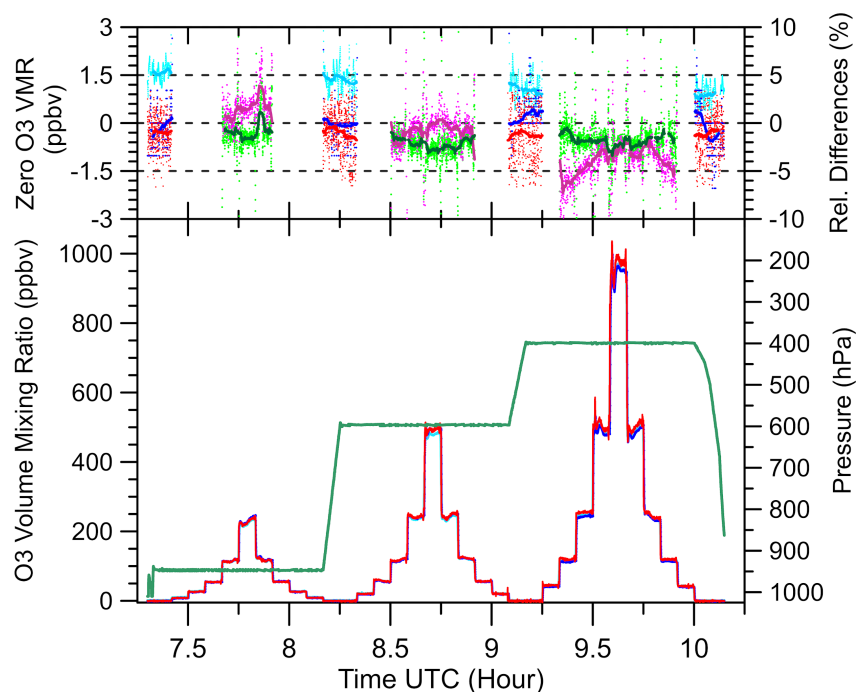


**Figure 9.** Experiment #7: colour coding as listed in Figure 4. In addition, in the upper panel (left vertical coordinate) are plotted the ozone offsets (red: OPM; blue: P1-O3; light blue: CAR-O3) measured during periods of zero ozone air, whereby fat solid lines are 3-minute running averages of the offsets.

At low pressure around 400 hPa (Fig. 9), P1-O3 shows a small ozone dependent bias to the OPM from -5 % at ~100 ppbv to -2% at ~1000 ppbv. The bias of CAR-O3 relative to OPM is again (as in Exp#3 and #4) around -(1-2) % and is constant over the entire pressure range of 400 - 1000 hPa with ozone volume mixing ratios up to 1000 ppbv. Although the three instruments follow the changes in ozone levels below 100 ppbv, only relative differences for the higher ozone levels are shown in Fig. 9. This to avoid that at lower ozone concentrations even small differences between the instruments can easily produce large relative values. Therefore, to compare the behaviour of P1-O3 and CAR-O3 in more detail, figure 10 shows ozone VMR scatter plots of P1-O3 versus OPM and CAR-O3 versus OPM, respectively, for the three discrete pressure levels of 950, 600 and 400 hPa, once for the full ozone ranges upper panel) and once for the lower ozone ranges (lower panel). The lower ozone VMR levels are more representative of tropospheric conditions (Fig. 10-d, e, f).

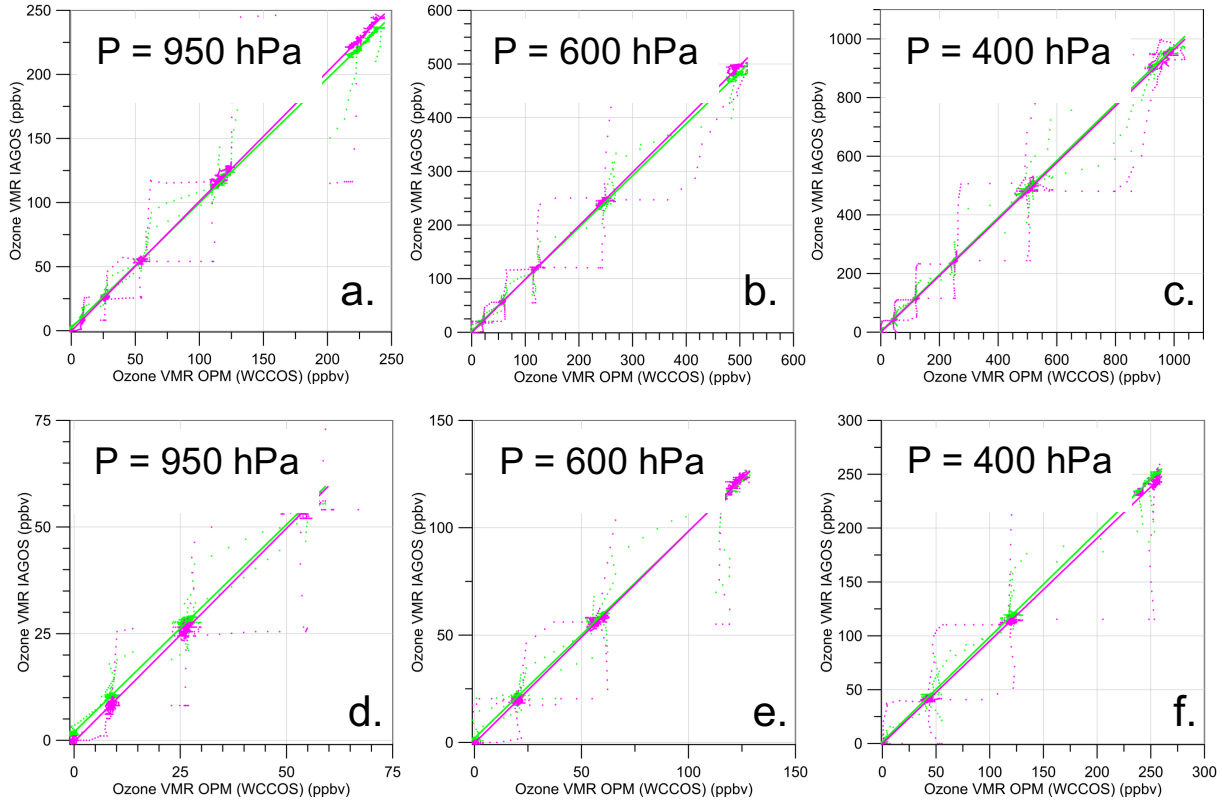


**Figure 10. Experiment #7: Ozone pressures measured by IAGOS instruments versus OPM at different ozone VMR levels (ppbv) for three discrete constant air pressure levels: 950, 600 and 400 hPa. Displayed are the scatter plots of P1-O3 versus OPM (Magenta) and CAR-O3 versus OPM (Green) and the solid straight lines are their linear fits through the origin. Upper panel displays the full ozone ranges (graphs a., b., c.) and the lower panel the lower ozone ranges (graphs d., e., f.) at the three different air pressure levels.**

The results for each pressure level (950, 600 and 400 hPa) are summarized in Table 3, once for the entire ozone VMR range and once for the lower ozone VMR level. The offsets of the instruments have been determined in the periods when measuring zero ozone air by averaging over 5 minute intervals (Fig.9: upper panel, left vertical coordinate). At each pressure level the slope has been derived from a linear curve fit of the scatter plots of P1-O3 and CAR-O3 versus OPM (Fig. 10). To investigate any hysteresis effect, the slopes have been determined also for the upward step ozone levels and downward step levels, the corresponding figures are shown in the supplementary material (Fig. S1 and Fig. S2 for P1-O3 and CAR-O3 against OPM, respectively). All results of slopes and offsets are summarized in Table 3.

From Table 3 it is seen that the behaviour between the three instruments observed at ozone levels larger than about 100 ppbv is consistent with the results obtained from the Exp. #3 and Exp. #4. At lower ozone values below 100 ppbv, however, the slopes for P1-O3/OPM differ slightly by  $\sim (1-2) \%$  compared to their corresponding slopes of P1-O3/OPM derived for higher ozone values, respectively. Breaking down the slopes into the upward and downward part of the ozone step levels, P1-O3/OPM reveals a small hysteresis effect of about 2 % which is most pronounced in the lower range of ozone levels. CAR-O3 shows no hysteresis, neither at the higher nor at the lower ozone levels (Table 3 and Figs. S1 and S2 in the supplement). The observed differences are not really understood but are still within the experimental reproducibility of about  $\pm 1 \%$  as mentioned in Section 3.2.2.



**Table 3. Offsets of OPM, P1-O3 and CAR-O3 determined from zero ozone air measurements (Fig.8) and slope of linear curve fits of scatter plots of P1-O3 and CAR-O3 versus OPM scatter plots (Fig.9), respectively, at three different air pressure levels: 950, 600 and 400 hPa for all data (Fig.9), included the corresponding slopes for the upward and downward ozone step levels, respectively (Fig. S1 and S2 in the supplementary material, respectively).**

Pressure (hPa)	Ozone Range (ppbv)	Ozone Data	P1-O3/OPM Slope	CAR-O3/OPM Slope	OPM Offset at zero O <sub>3</sub> (ppbv)	P1-O3 Offset at zero O <sub>3</sub> (ppbv)	CAR-O3 Offset at zero O <sub>3</sub> (ppbv)
950	0	Zero	--	--	-0.25±0.5	-0.30±0.6	1.5±0.2
	0-250	All	1.012	0.975	--	--	--
		Up	1.007	0.973	--	--	--
		Down	1.020	0.977	--	--	--
	0-75	All	1.002	0.973	--	--	--
		Up	0.980	0.971	--	--	--
		Down	1.023	0.976	--	--	--
600	0	Zero	--	--	-0.27±0.7	-0.08±0.3	1.5±0.3
	0-600	All	0.995	0.972	--	--	--
		Up	0.993	0.970	--	--	--
		Down	1.010	0.974	--	--	--
	0-150	All	0.986	0.971	--	--	--
		Up	0.975	0.968	--	--	--
		Down	0.990	0.974	--	--	--
400	0	Zero	--	--	-0.23±1.0	-0.32±0.6	1.1±0.5
	0-1100	All	0.964	0.975	--	--	--
		Up	0.958	0.970	--	--	--
		Down	0.972	0.978	--	--	--
	0-300	All	0.954	0.974	--	--	--
		Up	0.949	0.971	--	--	--
		Down	0.968	0.976	--	--	--

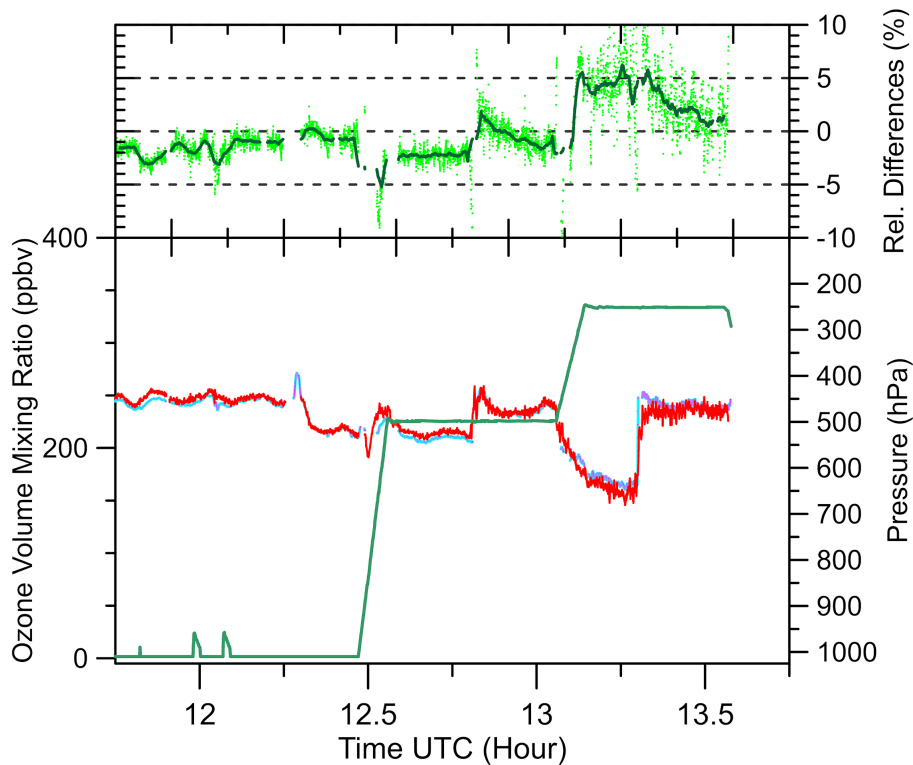
### 3.3 Comparison CAR-O3 Versus OPM at 250-1000 hPa Pressure

#### 3.3.1 Experiment #5: Discrete Pressure Levels (1000-250 hPa)

To simulate the real cruise altitude conditions for CAR-O3 (see section 2.3.2), a simulation experiment was repeated at three different pressure levels (1000, 500 and 250 hPa), whereby the ozone volume mixing ratios were kept at levels between 150 and 250 ppbv. The P1-O3 did not participate in this comparison experiment because the low-pressure level

447 of 250 hPa is not within the specification of the P1-Pump Box to operate against 1000 hPa laboratory pressure instead of  
 448 850 hPa cabin air (i.e., the pressure under real flight conditions, see section 2.3.2). In this simulation the total volume flow  
 449 rate of the OPS,  $\Phi_{OPS}$  is reduced to 12 vol-l/min. The results are shown in Figure 11.

450 At 1000 hPa and 500 hPa the results are very similar with the results of Exp.#3 and Exp. #4, while at 250 hPa initially  
 451 CAR-O3 shows slight enhanced values of about + (4-5) % compared to OPM, but after about 10 minutes, the difference  
 452 declined to + (1-2) %. The cause of this behaviour has been investigated by evaluating the housekeeping data of both  
 453 instruments (CAR-O3 and OPM) as well as the OPS and ESC; however, no indication of any malfunction of any of the  
 454 components could be detected. The cause is still not understood; it is a subject for further detailed investigations.



455  
 456 **Figure 11. Experiment #5: colour coding as listed in Figure 9.**

### 457 3.3.2 Experiment #6: Zero O3 Ascent (1000-180 hPa)

458 In this experiment the ascent pressure (down to 200 hPa) was simulated while ozone was kept at zero to measure the zero  
 459 signals of the CAR-O3 and OPM, while P1-O3 did not participate in the experiment. The OPM showed a small negative  
 460 offset about - (0.02-0.05 mPa), but a rather noisy signal, unrealistic high and most likely due to the enhanced temperatures  
 461 of the UV-light detector electronics exceeding the 50 °C threshold that occurred during the experiment. The CAR-O3  
 462 showed a small positive offset of 0.1 mPa at 1000 hPa that vanishes towards lower pressures, which agrees with results of  
 463 Exp.#7 (Table 3).

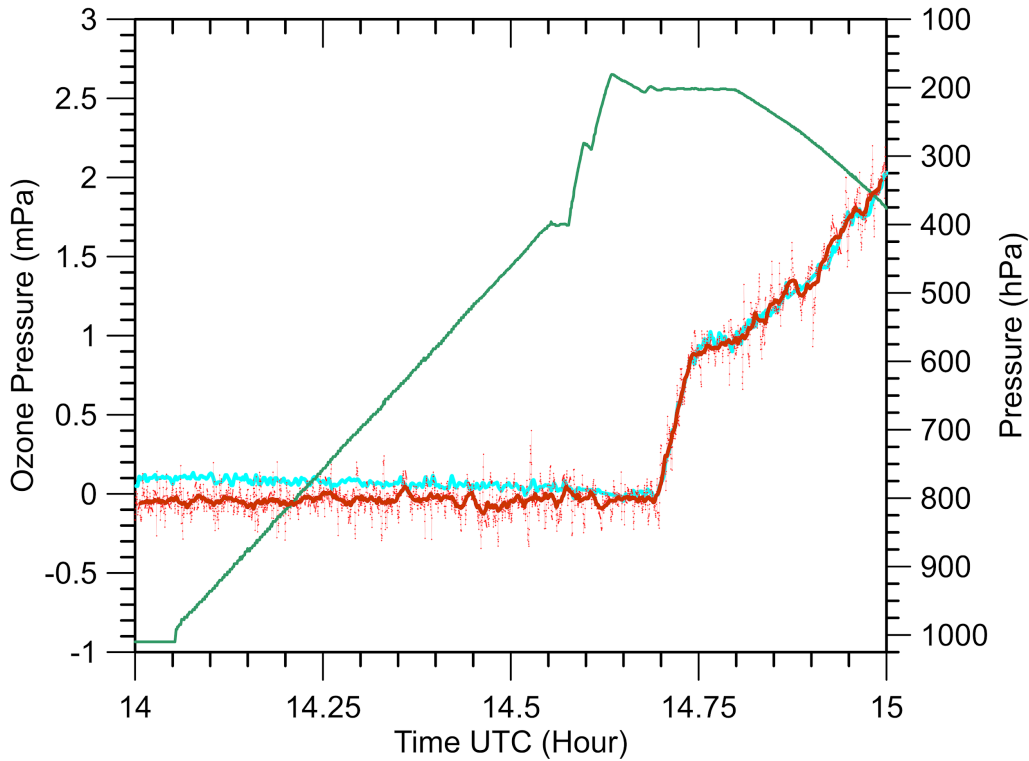


**Figure 12. Experiment #6: Time series of pressure (green) and ozone pressure (mPa) for CAR-O3 (light blue) and OPM (red), while ozone is kept initially at zero and after 14.70 (~14:42) ozone increased towards 2 mPa.**

#### 4. Discussion, Conclusions and Recommendations

In general, the IAGOS-O<sub>3</sub> instruments P1-O3 and CAR-O3 as well as the OPM showed consistent and good agreement among each other within a range better than about 5 %. CAR-O3 showed on average about -(1-2) % deviation to the OPM, but no clear pressure dependence within the 1000 hPa down to 400 hPa range, while at 250 hPa CAR-O3 showed about 2-4 % more ozone than the OPM. P1-O3 showed a good performance with a moderate increasing pressure dependent O<sub>3</sub> deviation to the OPM of about +2% at 1000 hPa to -3% at 400 hPa. The observed differences are small but systematic. The underlying causes should be better understood, also with respect to how far the observed results are consistent among the suite of instruments flown within IAGOS. Further, an experimental artefact of a few percent cannot be fully excluded, because we had to modify the WCCOS-JOSIE experimental setup to be able to adapt to the large sampling volume flow rate of about 24 l/min of the P1-O3 (Section 2.3.1). However, no indications are found on any memory or hysteresis effects for both instruments. For IAGOS-O<sub>3</sub> the long-term stability of the base line of the measured ozone records is extremely important to derive long term ozone changes of the order of one percent per decade.

Further, the intercomparison experiments here have shown that the reproducibility of the performance of the OPM as a standard, in combination with the experimental set up, within about  $\pm 1$  %. A primary standard for O<sub>3</sub>-UV photometer measuring only exists at Earth surface conditions, a primary standard exists at the Bureau International des Poids et Mesures (BIPM), Paris, France, but not for the free atmosphere or at reduced pressure. Therefore, even all intercomparisons in the past like JOSIE (comparison of ozonesondes against OPM) as well as this study (IAGOS-O<sub>3</sub> versus OPM) must be interpreted as being relative to each other. Hereby in this intercomparison the OPM acts as the

reference instrument. However, it is an important gap in doing intercomparison studies like this that no ozone reference instrument running at reduced pressures exists at any National Metrological Institute in the world. For the global observation networks of measuring free atmospheric ozone concentrations, it is crucial to close this gap to harmonize long term ozone records from different platforms (e.g. aircraft or balloon sondes) to one reference standard.

This intercomparison is a first step with the goal to get the global ozone sonde data (GAW-NDACC-SHADOZ-GRUAN) and IAGOS-O<sub>3</sub> (CORE & CARIBIC) data traceable to one common reference (OPM of WCCOS). While the aircraft and sonde measurements are often complementary, their records do not typically cover the same period. It is therefore essential to know and quantify potential biases and characteristics over time when merging their long-term records for process or trend studies. Tarasick et al. (2019) has evaluated earlier in-flight comparisons with ozonesonde measurements within a certain coincidence of space and time (Thouret et al., 1998; Staufer et al., 2013, 2014; Tanimoto et al., 2015) and found a consistent average relative positive bias of 5 % - 10 % between the ozonesondes and IAGOS. In a most recent study (Wang et al., 2024) has confirmed and discussed this observed bias, but no conclusive explanation could be given. It is known that ozone sondes in the troposphere can overestimate ozone by up to 5% (Smit et al., 2007, 2024; Thompson et al., 2019), while aircraft measurements may underestimate ozone due to wall losses when compressing the sampled air before measurement (Dias-Lalcaca et al., 1998; Brunner et al., 2001; Schnadt-Poberaj et al., 2007). However, this intercomparison study has shown that a freshly serviced Pump Box compressing the sampled air to cabin air pressure conditions, before entering the P1-O<sub>3</sub> monitor unit of P1-CORE-package, has only a small, in any, impact of less than 2-3% compared to the total measurement error. Further investigations on the performance of the Pump Boxes are needed, particularly the ones which have been flown during long periods of IAGOS-CORE flight operation and thus may have been exposed to highly polluted air masses containing contaminants (e.g. aerosols) near airports during take-off or landing of the aircraft. A key question thereby is: Can these contaminants have an impact on the performance of P1-O<sub>3</sub> or may the self-cleansing effect through high ozone concentrations, when flying in the stratosphere, be efficient enough that the impact is small or can be neglected?

A more regular validation of IAGOS-O<sub>3</sub> on external consistency is therefore essential and could be achieved by regular comparisons of the IAGOS-O<sub>3</sub> instruments together with ozonesondes against the OPM of the WCCOS in their environmental simulation chamber. This would be an important milestone in ozone research in the free troposphere and UTLS.

An important existing gap in doing intercomparison studies like this, however, is that no ozone reference instrument is running at reduced pressures at any National Metrological Institute in the world. For the global observation networks of measuring free atmospheric ozone, it is essential to close this gap in the future to enable the traceability of ozone measurements from different platforms to one reference standard, which is crucial to harmonize long-term ozone records and the detection of long term-changes in the free atmosphere.

## Acknowledgement

The WCCOS has been sponsored by the Forschungszentrum Jülich GmbH and WMO-GAW. IAGOS is supported by the European Commission, Airbus and the airlines (Deutsche Lufthansa, Air France, Austrian Airlines, Air Namibia, Cathay Pacific, Iberia, China Airlines, Hawaiian Airlines, and Air Canada so far) that have carried the MOZAIC or IAGOS

528 equipment and performed the maintenance since 1994. IAGOS has been funded by the European Union projects IAGOS-  
529 DS and IAGOS-ERI. Additionally, IAGOS has been funded by INSU-CNRS (France), Météo-France, Université Paul  
530 Sabatier (Toulouse, France) and Forschungszentrum Jülich GmbH. The IAGOS database is supported in France by AERIS  
531 (<https://www.aeris-data.fr>).

## 532 **Competing interests**

533 One of the co-authors Andreas Zahn is a member of the editorial board of Atmospheric Measurement Techniques. The  
534 peer review process will be guided by an independent editor. The authors have no other competing interests to declare.

## 535 **List of Acronyms**

536	<b>ASOPOS</b>	Assessment of Standard Operating Procedures for OzoneSondes
537	<b>CARIBIC</b>	Civil Aircraft for the Regular Investigation of the atmosphere Based on an Instrument Container
538	<b>CCQM-GAWG</b>	Consultative Committee for Amount of Substance: Metrology in Chemistry and Biology-
539		Gas Analysis Working Group
540	<b>CO</b>	Carbon monoxide
541	<b>DS</b>	Design Study
542	<b>ECC</b>	Electrochemical Concentration Cell
543	<b>ERI</b>	European Research Infrastructure
544	<b>ESC</b>	Environmental Simulation Chamber
545	<b>FTIR</b>	Fourier Transform Infra-Red spectroscopy
546	<b>FZJ</b>	ForschungsZentrum Jülich
547	<b>GAW</b>	Global Atmosphere Watch
548	<b>GCOS</b>	Global Climate Observing System
549	<b>GRUAN</b>	GCOS Reference Upper Air Network
550	<b>HALO</b>	High Altitude and Long-Range Research Aircraft
551	<b>IAGOS</b>	In-service Aircraft for a Global Observing System
552	<b>INSU</b>	Institut National des Sciences de l'Univers
553	<b>IPCC</b>	Intergovernmental Panel on Climate Change
554	<b>JOSIE</b>	Jülich OzoneSonde Intercomparison Experiment
555	<b>KIT</b>	Karlsruher Institut für Technologie
556	<b>LIDAR</b>	Light Detection and Ranging
557	<b>MOZAIC</b>	Measurement of OZone and water vapor by AIrbus in-service airCRAFT (now IAGOS)
558	<b>NDACC</b>	Network for the Detection of Atmospheric Composition Change
559	<b>OPM</b>	Ozone PhotoMeter instrument (used as UV-reference for ECC-ozonesondes at WCCOS)
560	<b>OPS</b>	Ozone Profile Simulator
561	<b>SHADOZ</b>	Southern Hemisphere ADditional OZonesonde
562	<b>SPARC</b>	Stratosphere-troposphere Processes And their Role in Climate
563	<b>STP</b>	Standard Temperature (=273.15 K) and Pressure (=1013.25 hPa) conditions
564	<b>TEI</b>	Thermo Environmental Instruments

565	<b>TOAR</b>	Tropospheric Ozone Assessment Report
566	<b>UNEP</b>	United Nations Environment Programme
567	<b>UTC</b>	Coordinated Universal Time
568	<b>UV</b>	Ultra-Violet
569	<b>VMR</b>	Volume Mixing Ratio
570	<b>WCCOS</b>	World Calibration Centre for OzoneSonde
571	<b>WMO</b>	World Meteorological Organization

572 **References**

573 Ancellet, A. and Ravetta, F.: Compact airborne lidar for tropospheric ozone: description and field measurements, *Appl.*  
574 *Opt.*, 37, 5509–5521, 1998.

575 Blot, R., Nédélec, P., Boulanger, D., Wolff, P., Sauvage, B., Cousin, J.-M., Athier, G., Zahn, A., Obersteiner, F., Scharffe,  
576 D., Petetin, H., Bennouna, Y., Clark, H., and Thouret, V.: Internal consistency of the IAGOS ozone and carbon monoxide  
577 measurements for the last 25 years, *Atmos. Meas. Tech.*, 14, 3935–3951, <https://doi.org/10.5194/amt-14-3935-2021>, 2021.

578 Brenninkmeijer C.A.M., P.J. Crutzen, T.Z. Immelmann, D. Kersting, M. Maiss, M. Nolle, A. Pitscheider, H. Pohlkamp, D.  
579 Scharffe, K. Specht, and A. Wiedensohler, CARIBIC - Civil aircraft for global measurement of trace gases and aerosols in  
580 the tropopause region, *J. Atmos. Ocean. Tech.*, 16, 1373-1383, 1999.

581 Brenninkmeijer, C.A.M., Crutzen, P., Boumard, F., Dauer, T., Dix, B., Ebinghaus, R., Filippi, D., Fischer, H., Franke, H.,  
582 Frieß, U., Heintzenberg, J., Helleis, F., Hermann, M., Kock, H. H., Koepfel, C., Lelieveld, J., Leuenberger, M., Martinsson,  
583 B. G., Miemczyk, S., Moret, H. P., Nguyen, H. N., Nyfeler, P., Oram, D., O'Sullivan, D., Penkett, S., Platt, U., Pupek, M.,  
584 Ramonet, M., Randa, B., Reichelt, M., Rhee, T. S., Rohwer, J., Rosenfeld, K., Scharffe, D., Schlager, H., Schumann, U.,  
585 Slemr, F., Sprung, D., Stock, P., Thaler, R., Valentino, F., van Velthoven, P., Waibel, A., Wandel, A., Waschitschek, K.,  
586 Wiedensohler, A., Xueref-Remy, I., Zahn, A., Zech, U., and Ziereis, H.: Civil Aircraft for the regular investigation of the  
587 atmosphere based on an instrumented container: The new CARIBIC system, *Atmos. Chem. Phys.*, 7, 4953–4976,  
588 <https://doi.org/10.5194/acp-7-4953-2007>, 2007.

589 Brunner, D., Staehelin, J., Jeker, D., Wernli, H., and Schumann, U.: Nitrogen oxides and ozone in the tropopause region  
590 of the Northern Hemisphere: Measurements from commercial aircraft in 1995/96 and 1997, *J. Geophys. Res.*, 106, 27673-  
591 27699, 2001.

592 CCQM-GAWG-2024/03: Guidelines how to implement the new absorption cross-section for ozone concentration  
593 measurements, <https://www.bipm.org/documents/d/guest/rapportbipm2024-03>, 2024.

594 Cohen, Y., Petetin, H., Thouret, V., Marécal, V., Josse, B., Clark, H., Sauvage, B., Fontaine, A., Athier, G., Blot, R.,  
595 Boulanger, D., Cousin, J.-M., and Nédélec, P.: Climatology and long-term evolution of ozone and carbon monoxide in  
596 the upper troposphere–lower stratosphere (UTLS) at northern midlatitudes, as seen by IAGOS from 1995 to 2013,  
597 *Atmos. Chem. Phys.*, 18, 5415–5453, <https://doi.org/10.5194/acp-18-5415-2018>, 2018.

598 Cooper, O.R., D.D. Parrish, J. Ziemke, N.V. Balashov, M. Cupeiro, I.E. Galbally, S. Gilge, L. Horowitz, N.R. Jensen, J.-  
599 F. Lamarque, V. Naik, S.J. Oltmans, J. Schwab, D.T. Shindell, A.M. Thompson, V. Thouret, Y. Wang, and R.M.

600 Zbinden: Global distribution and trends of tropospheric ozone: An observation-based review. *Elementa Sci.*  
 601 *Anthropocene*, 2, 000029, doi:10.12952/journal.elementa.000029, 2014

602 Dias-Lalcaca, P., Brunner, D., Imfeld, W., Moser, W., and Stachelin, J.: An Automated System for the Measurement of  
 603 Nitrogen Oxides and Ozone Concentrations from a Passenger Aircraft: Instrumentation and First Results of the NOXAR  
 604 Project, *Env. Sci. Tech.*, 32, 3228-3236, 1998.

605 Gaudel, A., Cooper, O.R., Chang, K.-L., Bourgeois, I., Ziemke, J.R., Strode, S.A., Oman, L.D., Sellitto, P., Nédélec, P.,  
 606 Blot, R., Thouret, V. & Granier, C.: Aircraft observations since the 1990s reveal increases of tropospheric ozone at multiple  
 607 locations across the Northern Hemisphere. (Vol. 6). <https://doi.org/10.1126/sciadv.aba8272>, 2020.

608 Petetin, H., Thouret, V., Athier, G., Blot, R., Boulanger, D., Cousin, J.-M., Gaudel, A., Nédélec, P. & Cooper, O.: Diurnal  
 609 cycle of ozone throughout the troposphere over Frankfurt as measured by MOZAIC-IAGOS commercial aircraft. (Vol. 4).  
 610 <https://doi.org/10.12952/journal.elementa.000129>, 2016.

611 Hearn, A.G.: Absorption of ozone in ultra-violet and visible regions of spectrum, *Proc. Phys. Soc.*, 78, 932–940, 1961.

612 Hodges, J.T., Viallon, J., Brewer, P.J., Drouin, B.J., Gorshelev, V., Janssen, C., Lee, S., Possolo, A., Smith, M.A.H.,  
 613 Walden, J., Wielgosz, R.I.: Recommendation of a consensus value of the ozone absorption cross-section at 253.65 nm  
 614 based on a literature review, *Metrologia*. 56: 034001. <https://iopscience.iop.org/article/10.1088/1681-7575/ab0bdd>, 2019

615 Hu, L., Jacob, D.J., Liu, X., Zhang, Y., Zhang, L., Kim, P.S., Sulprizio, M.P., Yantosca, R.M.: Global budget of  
 616 tropospheric ozone: Evaluating recent model advances with satellite (OMI), aircraft (IAGOS), and ozonesonde  
 617 observations, *Atm. Env.*, 167, 323-334, <https://doi.org/10.1016/j.atmosenv.2017.08.036>, 2017.

618 IPCC-Climate Change: The Physical Science Basis. Contribution of Working Group I to the Sixth Assessment Report of  
 619 the Intergovernmental Panel on Climate Change, edited by: Masson-Delmotte, V., Zhai, P., Pirani, A., Connors, S.L., Péan,  
 620 C., Berger, S., Caud, N., Chen, Y., Goldfarb, L., Gomis, M. I., Huang, M., Leitzell, K., Lonnoy, E., Matthews, J. B. R.,  
 621 Maycock, T. K., Waterfield, T., Yelekçi, O., Yu, R., and Zhou, B., Cambridge University Press, Cambridge, United  
 622 Kingdom and New York, NY, USA, in press, <https://doi.org/10.1017/9781009157896>, 2023.

623 Marengo, A., V. Thouret, P. Nédélec, H. Smit, M. Helten, D. Kley, F. Karcher, P. Simon, K. Law, J. Pyle, G. Poschmann,  
 624 R. Von Wrede, C. Hume and T. Cook: Measurement of ozone and water vapor by Airbus in-service aircraft: The MOZAIC  
 625 airborne program, An overview, *J. Geophys. Res.*, 103, 25,631-25,642, 1998.

626 McDermid, I. S., Haner, D. A., Kleiman, M. M., Walsh, T. D., and White, M. L.: Differential absorption lidar systems for  
 627 tropospheric and stratospheric ozone measurements, *Opt. Engin.*, 30, 22–30, 1991.

628 Nédélec P., Blot R., Boulanger D., Athier G., Cousin J.-M., Gautron B., Petzold A., Volz-Thomas A. and Thouret V.,  
 629 Instrumentation on commercial aircraft for monitoring the atmospheric composition on a global scale: the IAGOS system,  
 630 technical overview of ozone and carbon monoxide measurements, MOZAIC-IAGOS special issue, *Tellus B* 2015, 67,  
 631 27791, <http://dx.doi.org/10.3402/tellusb.v67.27791>.

632 Obersteiner, F.: FAIROmeta (v0.1.8), <https://doi.org/10.5281/zenodo.11104076>, 2024.

633 Petzold A., V. Thouret, C. Gerbig, A. Zahn, C.A.M. Brenninkmeijer, M. Gallagher, M. Hermann, M. Pontaud, H. Ziereis,  
 634 D. Boulanger, J. Marshall, P. Nédélec, H.G.J. Smit, U. Frieß, J.-M. Flaud, A. Wahner, J.-P. Cammas, A. Volz-Thomas,

635 and IAGOS Team: Global-Scale Atmosphere Monitoring by In-Service Aircraft - Current Achievements and Future  
636 Prospects of the European Research Infrastructure IAGOS, *Tellus-B*, 67, 28452. doi:10.3402/tellusb.v67.28452, 2015.

637 Petzold, A., Bundke, U., Hienola, A., Laj, P., Lund Myhre, C., Vermeulen, A., Adamaki, A., Kutsch, W., Thouret, V.,  
638 Boulanger, D., Fiebig, M., Stocker, M., Zhao, Z., and Asmi, A.: Opinion: New directions in atmospheric research offered  
639 by research infrastructures combined with open and data-intensive science, *Atmos. Chem. Phys.*, 24, 5369–5388,  
640 <https://doi.org/10.5194/acp-24-5369-2024>, 2024.

641 Proffitt, M.H. and McLaughlin, R.J.: Fast response dual-beam UV-absorption photometer suitable for use on stratospheric  
642 balloons, *Rev. Sci. Instr.*, 54, 1719–1728, 1983.

643 Schnadt Poberaj, C., Staehelin, J., Brunner, D., Thouret, V., and Mohnen, V.: A UT/LS ozone climatology of the nineteen  
644 seventies deduced from the GASP aircraft measurement program, *Atmos. Chem. Phys.*, 7, 5917–5936,  
645 <https://doi.org/10.5194/acp-7-5917-2007>, 2007.

646 Schneider, M., Blumenstock, T., Hase, F., Höpfner, M., Cuevas, E., Redondas, A., and Sancho, J. M.: Ozone profiles and  
647 total column amounts derived at Izana Tenerife Island, from FTIR solar absorption spectra, and its validation by an  
648 intercomparison to ECC-sonde and Brewer spectrometer measurements, *J. Quant. Spectros. Radiat. Transfer*, 245-274,  
649 <https://doi.org/10.1016/j.jqsrt.2004.05.067>, 2005.

650 Smit H.G.J., Sträter, W., Helten, M. and Kley, D.: Environmental Simulation Facility to Calibrate Airborne Ozone and  
651 Humidity Sensors. Jül Berichte, No. 3796, Forschungszentrum Jülich, 2000.

652 Smit, H. G. J., Sträter, W., Johnson, B. J., Oltmans, S. J., Davies, J., Tarasick, D. W., Högger, B., Stübi, R., Schmidlin, F.  
653 J., Northam, T., Thompson, A. M., Witte, J. C., Boyd, I., and Posny, F.: Assessment of the performance of ECC  
654 ozonesondes under quasi-flight conditions in the environmental simulation chamber: Insights from the Jülich Ozone Sonde  
655 Intercomparison Experiment (JOSIE), *J. Geophys. Res.*, 112, D19306, <https://doi.org/10.1029/2006JD007308>, 2007.

656 Smit, H. G. J., Thompson, A. M., and the ASOPOS 2.0 Panel: Ozonesonde Measurement Principles and Best Operational  
657 Practices, WMO Global Atmosphere Watch Report Series, No. 268, World Meteorological Organization, Geneva,  
658 <https://library.wmo.int/idurl/4/57720> (last access: 10 December 2023), 2021.

659 Smit, H. G. J., Poyraz, D., Van Malderen, R., Thompson, A.M., Tarasick, D. W., Stauffer, R. M., Johnson, B. J., and  
660 Kollonige, D. E.: New insights from the Jülich Ozone Sonde Intercomparison Experiment: calibration functions traceable  
661 to one ozone reference instrument, *Atmos. Meas. Tech.*, 17, 73–112, <https://doi.org/10.5194/amt-17-73-2024>, 2024.

662 Staufer, J., Staehelin, J., Stübi, R., Peter, T., Tummon, F., and Thouret, V.: Trajectory matching of ozonesondes and  
663 MOZAIC measurements in the UTLS - Part 1: Method description and application at Payerne, Switzerland. *Atmos. Meas.*  
664 *Tech.*, 6, 3393-3406, doi:10.5194/amt-6-3393-2013, 2013.

665 Staufer, J., Staehelin, J., Stübi, R., Peter, T., Tummon, F., and Thouret, V.: Trajectory matching of ozonesondes and  
666 MOZAIC measurements in the UTLS - Part 2: Application to the global ozonesonde network. *Atmos. Meas. Tech.*, 7, 241-  
667 266, doi:10.5194/amt-7-241-2014, 2014.

668 Tarasick, D., Galbally, I.E., Cooper, O.R., Schultz, M.G., Ancellet, G., Leblanc, T., Wallington, T.J., Ziemke, J., Liu, X.,  
669 Steinbacher, M., Staehelin, J., Vigouroux, C., Hannigan, J.W., García, O., Foret, G., Zanis, P., Weatherhead, E.,  
670 Petropavlovskikh, I., Worden, H., Osman, M., Liu, J., Chang, K.-L., Gaudel, A., Lin, M., Granados-Muñoz, M., Thompson,



671 A.M., Oltmans, S.J., Cuesta, J., Dufour, G., Thouret, V., Hassler, B., Trickl, T. and Neu, J.L.: Tropospheric Ozone  
 672 Assessment Report: Tropospheric ozone from 1877 to 2016, observed levels, trends and uncertainties. *Elementa: Science*  
 673 *of the Anthropocene*, 7:39. <https://doi.org/10.1525/elementa.376>, 2019.

674 Tanimoto, H., Zbinden, R.M., Thouret, V., and Nédélec, P.: Consistency of tropospheric ozone observations made by  
 675 different platforms and techniques in the global databases, *Tellus B*, 67, 27073, <https://doi.org/10.3402/tellusb.v67.27073>,  
 676 2015.

677 Thompson, A.M., The oxidizing capacity of the earth's atmosphere: Probably past and future changes, *Science*, 256, 1157-  
 678 1165, 1992.

679 Thouret, V., A. Marenco, J. A. Logan, P. Nédélec, and C. Grouhel, Comparisons of ozone measurements from the  
 680 MOZAIC airborne program and the ozone sounding network at eight locations, *J. Geophys. Res.*, 103, 25,695-25,720,  
 681 1998.

682 Vigouroux, C., De Mazière, M., Demoulin, P., Servais, C., Hase, F., Blumenstock, T., Kramer, I., Schneider, M., Mellqvist,  
 683 J., Strandberg, A., Velasco, V., Notholt, J., Sussmann, R., Stremme, W., Rockmann, A., Gardiner, T., Coleman, M., and  
 684 Woods, P.: Evaluation of tropospheric and stratospheric ozone trends over Western Europe from ground-based FTIR  
 685 network observations, *Atmos. Chem. Phys.*, 8, 6865–6886, <https://doi.org/10.5194/acp-8-6865-2008>, 2008.

686 Wagner, A., Bennouna, Y., Blechschmidt, A.-M., Brasseur, G., Chabrillat, S., Christophe, Y., Errera, Q., Eskes, H.,  
 687 Flemming, J., Hansen, K.M., Inness, A., Kapsomenakis, J., Langerock, B., Richter, A., Sudarchikova, N., Thouret, V. &  
 688 Zerefos, C. (2021). Comprehensive evaluation of the Copernicus Atmosphere Monitoring Service (CAMS) reanalysis  
 689 against independent observations. (Vol. 9). <https://doi.org/10.1525/elementa.2020.00171>

690 Wang, H., Lu, X., Jacob, D.J., Cooper, O.R., Chang, K.-L., Li, K., Gao, M., Liu, Y., Sheng, B., Wu, K., Wu, T., Zhang, J.,  
 691 Sauvage, B., Nédélec, P., Blot, R. & Fan, S. (2022). Global tropospheric ozone trends, attributions, and radiative impacts  
 692 in 1995–2017: an integrated analysis using aircraft (IAGOS) observations, ozonesonde, and multi-decadal chemical model  
 693 simulations. (Vol. 22, pp. 13753-13782). <https://doi.org/10.5194/acp-22-13753-2022>

694 Wang, H., Tarasick, D.W., Liu, J., Smit, H.G.J., Van Malderen, R., Shen, L., Blot, R., and Zhao, T.: Consistency evaluation  
 695 of tropospheric ozone from ozonesonde and IAGOS (In-service Aircraft for a Global Observing System) observations:  
 696 vertical distribution, ozonesonde types, and station–airport distance, *Atmos. Chem. Phys.*, 24, 11927–11942,  
 697 <https://doi.org/10.5194/acp-24-11927-2024>, 2024.

698 Wilson, K.L. and Birks, J.W.: Mechanism and Elimination of a Water Vapor Interference in the Measurement of Ozone  
 699 by UV Absorbance, *Env. Sci. Tech.*, 40 (20), 6361-6367, DOI: 10.1021/es052590c, 2006.

700 WMO/UNEP: Scientific Assessment of Ozone Depletion: 2022, Ozone Research and Monitoring, GAW Report No. 278,  
 701 World Meteorological Organization, Geneva, ISBN: 978-9914-733-97-6, <https://library.wmo.int/idurl/4/58360> (last  
 702 access: 10 December 2023), 2023.

703 Zahn, A.: Standard Operating Procedure (SOP) of the IAGOS-CARIBIC Ozone Instrument, IAGOS-Technical Document,  
 704 2016.

705